ACS APPLIED MATERIALS & INTERFACES

Letter

www.acsami.org

Plasmonic Nanoantenna Arrays for Surface-Enhanced Raman Spectroscopy of Lipid Molecules Embedded in a Bilayer Membrane

Paul Kühler, Max Weber, and Theobald Lohmüller*

Photonics and Optoelectronics Group, Department of Physics and Center for NanoScience (CeNS), Ludwig Maximilian University München, Amalienstrasse 54, Munich 80799, Germany

Supporting Information

ABSTRACT: We demonstrate a strategy for surface-enhanced Raman spectroscopy (SERS) of supported lipid membranes with arrays of plasmonic nanoantennas. Colloidal lithography refined with plasma etching is used to synthesize arrays of triangular shaped gold nanoparticles. Reducing the separation distance between the triangle tips leads to plasmonic coupling and to a strong enhancement of the electromagnetic field in the nanotriangle gap. As a result, the Raman scattering intensity of molecules that are located at this plasmonic "hot-spot" can be increased by several orders of magnitude. The nanoantenna array is then embedded with a supported phospholipid membrane which is fluid at room temperature and spans the antenna gap. This configuration offers the advantage that molecules that are mobile within the bilayer membrane can enter the "hot-spot" region via diffusion and can therefore be measured by SERS without static entrapment or adsorption of the molecules to the antenna itself.

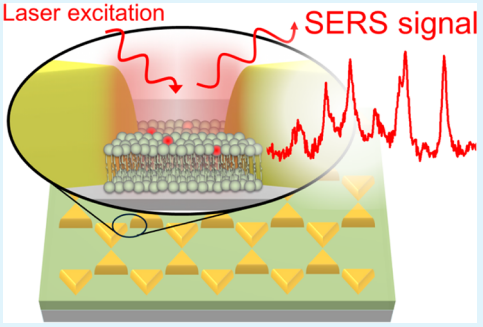

KEYWORDS: *lipid molecules, plasmonic nanoantennas, SERS, colloid lithography*

Biological membranes and their components such as lipid molecules and proteins are of functional importance for cells to communicate and interact with their environment.[1] Also, the structural and chemical interplay between individual molecules is crucial for many biochemical processes that take place on the cell membrane itself.[2] Studying membranes on a molecular level, however, is challenging because of their dynamic nature, heterogeneity, and small thickness.[3] Usually, membranes are studied by fluorescence-based methods, such as total internal reflection (TIR) fluorescence microscopy,[4] fluorescence interference contrast microscopy,[5] Förster resonance energy transfer,[6] or fluorescence correlation spectroscopy,[7] some of which provide even single molecule sensitivity. In general, however, these methods provide only limited information about the chemical fingerprint of the bilayer membrane or its membrane components. Other techniques such as secondary ion mass spectroscopy (SIMS) or nanoSIMS have been shown to be capable of performing an analysis of the elemental and molecular composition of cells and cell membranes with high special resolution.[8] However, these methods require ultrahigh vacuum conditions and are therefore not compatible with measurements in water, which is a prerequisite for imaging and spectroscopy on lipid membranes under physiological conditions.

Vibrational spectroscopy methods, such as infrared (IR) and Raman spectroscopy, are advantageous when it comes to identifying the structure and chemistry of membrane components.[9] In particular Raman spectroscopy, which is also suitable for measurements in water, has proven to be a powerful tool for measurements on biological samples. Raman signals arise from distinct vibrational energy levels of a molecule and each spectrum contains information about the chemical fingerprint of a sample, i.e., the structure of molecular constituents, intermolecular interactions, and conformational changes of the analyte.[10] Limitations for a wider use of this technique arise from the fact that the Raman scattering cross-sections of most molecules are usually very small and on the order of only 1×10^{-29} to 1×10^{-30} cm^2/molecule.[11] Acquiring spectral information from only a few molecules that are dispersed in a nanometer thin sample, such as a lipid membrane, is therefore challenging.

Several approaches have been reported in the past to perform Raman spectroscopy of phospholipid membranes including TIR Raman measurements.[12] Here, the sample was excited by the evanescent field of a totally reflected laser beam in order to increase the signal contribution from the bilayer membrane and to reduce the background noise at the same time. A 60-fold enhancement of the Raman signal was observed at acquisition times of a few minutes which is considerably shorter compared to acquisition times of 2 h, which were reported before for Raman studies on black membranes using standard confocal Raman microscopy.[13]

The TIR approach allowed for recordings of the whole membrane at once. The detection of a few molecules that are sparsely distributed across the bilayer membrane is significantly more challenging due to the low concentration of molecules

Received: April 17, 2014
Accepted: June 4, 2014
Published: June 4, 2014

   dx.doi.org/10.1021/am5023418 | *ACS Appl. Mater. Interfaces* 2014, 6, 8947−8952

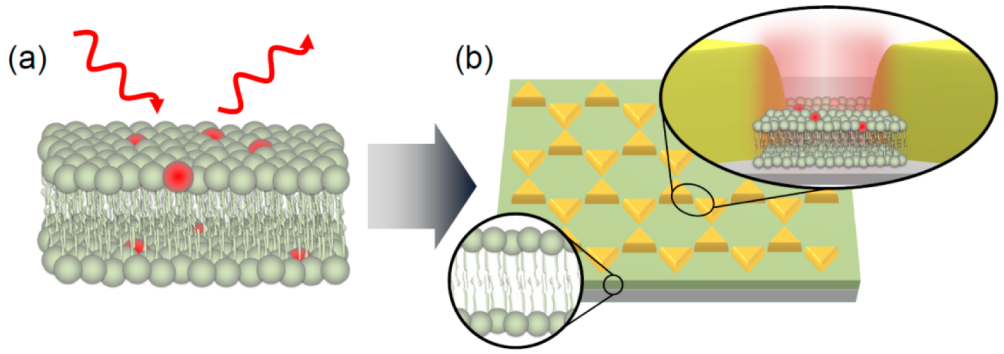

Figure 1. Schematic presentation of the experimental approach: (a) Lipids (with polar headgroup and nonpolar tail) forming a bilayer segment with a small fraction of molecules of interest (red). (b) Combination of plasmonically coupled nanotriangles with a fluid lipid membrane on a solid support. Laser illumination near the LSP resonance gives rise to a strong field enhancement between the tips of adjacent triangles, which can be employed for SERS measurements.

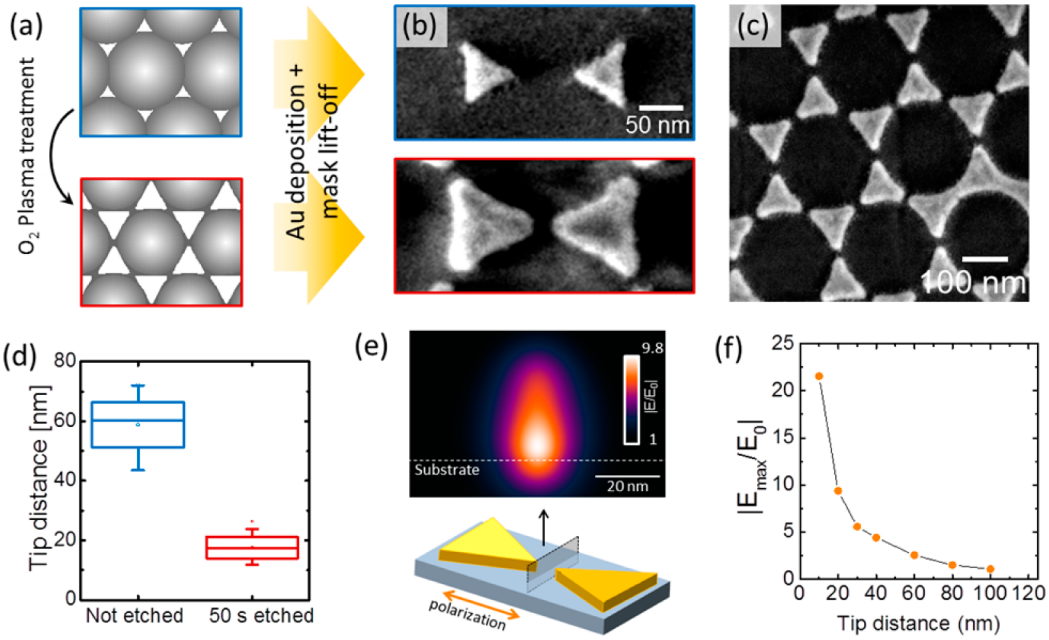

Figure 2. Fabrication of the nanoantenna array and simulations of its plasmonic properties. (a) Sketch of the hexagonal PS particle mask before (blue frame) and after (red frame) plasma treatment. (b) SEM close-up of Au nanotriangles resulting from gold evaporation on the nonetched (blue frame) and 50 s etched (red frame) PS particle mask. (c) SEM image of the nanotriangle array resulting from evaporating gold on a 50 s etched PS particle mask. (d) Statistical box plot of the distribution of tip distances for different etching times. (e) Calculated intensity of the electromagnetic field at the center of a nanoantenna gap. Simulations were performed for a wavelength λ = 647 nm, assuming glass as a substrate. The triangle height was set to be 30 nm, the side length 90 nm and the tip distance 20 nm. (f) Electromagnetic field enhancement in the center gap region (as indicated in e) as a function of the tip-to-tip distance. The line is a guide to the eye.

and would therefore require much longer acquisition times and/or high laser intensities. In principle though, short acquisition times are desired to account for the dynamic nature of lipid membranes and the mobility of lipid molecules which display lateral diffusion coefficients that are typically on the order of a few $\mu m^2/s$.[14]

Such a strong enhancement of the Raman scattering could be achieved by using plasmonic nanoantennas.[15] If two particles are brought in close proximity, the coupling between the localized surface plasmons (LSP) can generate a strongly enhanced, localized electric field or so-called plasmonic "hot-spot".[16] In the "hot-spot" region, the Raman scattering intensity is amplified by several orders of magnitude.[17] The molecules, however, need to be positioned precisely in the area of strongest coupling, which is in the gap between the two adjacent plasmonic particles. Ideally, for any measurement of a lipid bilayer the membrane would span the nanoantenna gap in order to benefit the most from the field enhancing effect.

An experimental tool to resemble the properties of a cell membrane on a solid support is a planar supported lipid bilayer (SLB).[18] An SLB can be formed on top of a hydrophilic glass slide via fusion of small unilamellar vesicles of phospholipid molecules within minutes.[19] But more importantly, SLBs can also be embedded with metallic nanostructures which allows to direct the lipid mobility while the fluidity of the bilayer membrane itself is preserved.[20−22] This has been successfully demonstrated for quantitative investigations of living cells where metal structures made of gold or chromium were applied as diffusion barriers to direct the movement of molecules in the membrane of living cells.[20,23] Experiments have also shown that the membrane molecules remain fluid, even at a very close distance to the metal edge and that single molecules are able to

diffuse through nanogate architectures that are as small as 10 nm.[24] This is an important observation, because molecules that are adsorbed to the metal barrier would lose their dynamic property, which is fundamental to the membrane function.

In this report, we demonstrate how phospholipid membranes embedded with plasmonic nanoantennas can be used to perform surface enhanced Raman spectroscopy (SERS) of molecules attached to a fluid bilayer membrane. This was realized by forming a single SLB doped with a 1% fraction of Rhodamine-B (RhB) labeled lipids in between an array of triangular shaped nanoantennas. The SERS signal of RhB is recorded as the lipids diffuse on the membrane and pass the hot-spot region between two nanoparticle tips (Figure 1). The fluid properties of the membrane are thereby utilized to transport the molecules of interest directly to the position of the highest field enhancement and the strongest Raman signal enhancement between the nanoantenna tips. Finally, the homogeneous enhancement of the Raman signal over a large surface area is demonstrated by confocal Raman-mapping of the membrane/nanoantenna interface.

Colloid lithography was used to generate a large array of bowtie shaped nanoantennas on top of a glass substrate. The general method for colloid lithography has been pioneered by Fisher and Zingsheim,[25] as well as Hulteen and van Duyne,[26] and has since been used by numerous research groups to generate arrays of plasmonic nanoparticles. Briefly, spherical polystyrene (PS) particles are self-assembled into a monolayer on a water surface which is transferred to a glass substrate. The monolayer then serves as shadow mask to evaporate a 30 nm thin film of gold on top. Finally, the colloid mask is removed and an array of gold nanotriangles is left behind on the glass surface. We would like to remark that despite its generally slightly smaller SERS performance compared to silver, we chose gold as material for the nanoantennas to avoid unwanted oxidation effects of the silver nanoparticles.

Several geometrical factors of the nanotriangle array have to be controlled and adjusted to optimize their applicability for SERS measurements: The particle size, which directly determines the wavelength of the localized plasmon resonance of the array, and the interparticle tip distance (or gap size). Ideally the distance between two particle tips must be reduced to only a few nanometers in the whole array to achieve the strongest plasmonic coupling and thus create an array of plasmonic "hot-spots". Controlling the triangle size and thickness is achieved straightforward by using smaller or bigger colloid particles to form the evaporation mask and to control the thickness of the evaporated gold film. Changing the tip-to-tip distance between all triangles homogeneously, however, requires further processing of the PS particle mask.[22] For this, an additional plasma step was added to the standard fabrication protocol (Figure 2a). We observed that plasma treatment has two effects on the particle mask. First, the diameter of the colloid spheres is reduced and second, small connecting threads are formed between neighboring colloids (Figure 2a) which result in a reduced separation distance of the gold nanotriangles array when used as a shadow mask.

We used PS spheres with a mean diameter of 250 nm in that way to generate a large array of nanoparticle triangles on top of a glass coverslip. Without additional plasma treatment, the triangles had a size of 58 nm (tip to base) and a plasmon extinction maximum at λ = 704 nm. The same colloid monolayer was exposed to oxygen plasma for 50s. The resulting nanoparticles were now bigger with a size of 83 nm (tip to base) and the interparticle tip distance was reduced at the same time to an average of ∼20 nm. As a consequence, the plasmon extinction maximum was also red-shifted to λ= 740 nm (see the Supporting Information, Figure S1). A direct comparison of the mean tip distance with and without plasma treatment is shown in Figure 2d. Without plasma treatment, the mean tip distance was 60 nm. After 50 s of plasma treatment the average tip-to-tip distance was found to be reduced by a factor of 3. The average gap size between the particles was now only 18 nm with about 25% of the gaps being smaller than 15 nm.

The plasma modification gives control over the gap size of the resulting bowties, which is of great importance for their plasmonic behavior. Finite-difference time-domain (FDTD) calculations were employed to calculate the distribution of the electric field enhancement $|E/E_0|$ in a single Au bowtie under illumination, with E and E_0 being the amplitudes of the local field and the incident electric field, respectively. Considering the application of SERS on supported membranes, we were particularly interested in the gap region between the tips of two opposing triangles. Analyzing the field distribution reveals that $|E_{max}/E_0|$ is located only 4.8 nm above the substrate surface (Figure 2e), indicating that the nanoantenna geometry is ideally suited for the purpose of SERS in a bilayer membrane with a thickness of approximately 5 nm.[27]

Figure 2f shows a strong increase of the maximum electric field enhancement $|E_{max}/E_0|$ at the gap center for decreasing tip-to-tip distance, which demonstrates the importance of controlling the size of the nanoantenna gap and agrees well with the findings for similar structures.[15,28] When comparing the values for the measured mean tip distances of the experimentally realized bowtie arrays (Figure 2c), one finds a 3.7-fold increase of $|E_{max}/E_0|$ for the reduced gap size from 60 to 20 nm (i.e., resulting from the etching process). Because the Raman enhancement scales with $|E|^4$ this increases the calculated SERS signal by a factor of 2×10^2 compared to the case without etching.[29] Furthermore, $|E/E_0|$ = 9.4 for a tip distance of 20 nm leads to a calculated (electromagnetic) SERS enhancement of $\sim 10^4$ at the gap center. For a precise calculation for a specific emission line, however, the Stokes shift of the emitted light has to be taken into account. The total gap region can be expected to yield an even higher SERS enhancement because the electric field enhancement increases toward the edge of the triangles. All molecules that are present at the gap will therefore experience a strong Raman signal enhancement.

Next, a SLB membrane was formed on the bare glass substrate in between the nanoantenna array. SLB were formed according to the protocol by Lin et al.[19] The lipid vesicles were made of 99 mol % unlabeled DOPC (1,2-dioleoyl-*sn*-glycero-3-phosphocholine) doped with 1 mol % of Rhodamine labeled lipids (18:1 LISS Rhod PE (L-RhB)) that served as Raman dye. Membranes of DOPC are fluid at room temperature and this fluidity is preserved when the bilayer is supported by a glass substrate. On the integrated nanoantenna/SLB platform, the gold triangles act as diffusion barriers.[21,22,20] Lipid molecules in the SLB are therefore not able to diffuse across the antennae because no fluid membrane will form on top of them. Instead, they will diffuse around the Au triangles, thereby sequentially passing a number of plasmonic "hot-spot". There they are exposed to the strong field enhancement in the nanoantenna gap which can be used to detect their SERS signal.[30]

SERS measurements on the nanoantenna/SLB platform were performed to demonstrate the capability of this approach to

detect a small fraction of freely diffusing membrane molecules. The fluidity of the membrane around the nanoantenna arrays was confirmed by photobleaching and fluorescence recovery of RhB lipid prior to SERS measurements (see the Supporting Information, Figure S2). From this measurement, we calculated a diffusion coefficient of 0.2 $\mu m^2/s$ for the membrane in between the triangle array, which is comparable to the diffusion coefficient of proteins in native cell membranes.[31] Even within a time period of several seconds, individual molecules are therefore likely to pass only a few gaps considering the length scale of the nanoantenna array. The 647 nm laser line of an argon/krypton laser was used for Raman excitation, which is far from the absorption peak of L-RhB (centered at 560 nm, width ~20 nm fwhm). This way, we could exclude that benefits from resonant Raman excitation contribute to the overall Raman signal. Furthermore, the laser excitation power density was set to only 80 $\mu W/\mu m^2$ in order to minimize the risk of photobleaching of the Rhodamine (for details about experimental configuration, see the Supporting Information, Figure S3).

An average of the single spectra was taken to further analyze the Raman spectrum (Figure 3). Corresponding averages of Raman maps on regions of the bare glass substrate as well as on a continuous gold film on the same sample show no distinct Raman peaks (see the Supporting Information, Figure S4). This demonstrates the significance of the triangle array for the Raman measurement in the membrane. The SERS spectrum was compared to a control measurement of L-RhB-lipids in bulk solution to determine the origin of the Raman peaks in the SLB spectra. Both spectra show very good agreement of the peak positions as well as the relative peak intensities between the regular Raman and SERS measurement. Furthermore, comparison of the peak positions to literature values (see Table 1) confirmed most peaks to be assigned exclusively to RhB (including the peak at 1530 cm^{-1} that was used to calculate the SERS enhancement).

Figure 4a shows an optical bright-field image of the substrate that supports the lipid membrane. The strongly scattering triangle array appears red, whereas the dark region indicates bare glass surface. Single-point SERS spectra that were mapped on the triangle array are shown in Figure 3b. The presented spectral region contains the most distinctive RhB Stokes peaks. SERS enhancement factors were calculated by comparing the intensity of the RhB peak at 1530 cm^{-1} measured on the SLB and compared to a bulk solution of SUVs consisting of pure L-RhB, which allows plotting a SERS map corresponding to the measured area (Figure 4b). It illustrates the homogeneity of the SERS enhancement over a large area. The nanotriangle array yields an average enhancement of 1.9×10^4, which represents the average over the gap region. An even larger SERS enhancement can be expected if the Raman excitation wavelength would better match the LSP resonance of the bowtie array.

For an accurate comparison with our calculations, we evaluated the calculated electric field enhancement at both the excitation wavelength and the emission wavelength which is Stokes-shifted to 718 nm. Our simulations thus yield an estimate for the enhancement factor of $(|E/E_0|^{(647)}|E/E_0|^{(718)})^2 = 2.9 \times 10^4$, which is in good agreement with the measured data.

Additional factors influencing the SERS performance are structural defects and the nanoantenna orientation. Approximately 90 gaps are probed at once at each measurement point

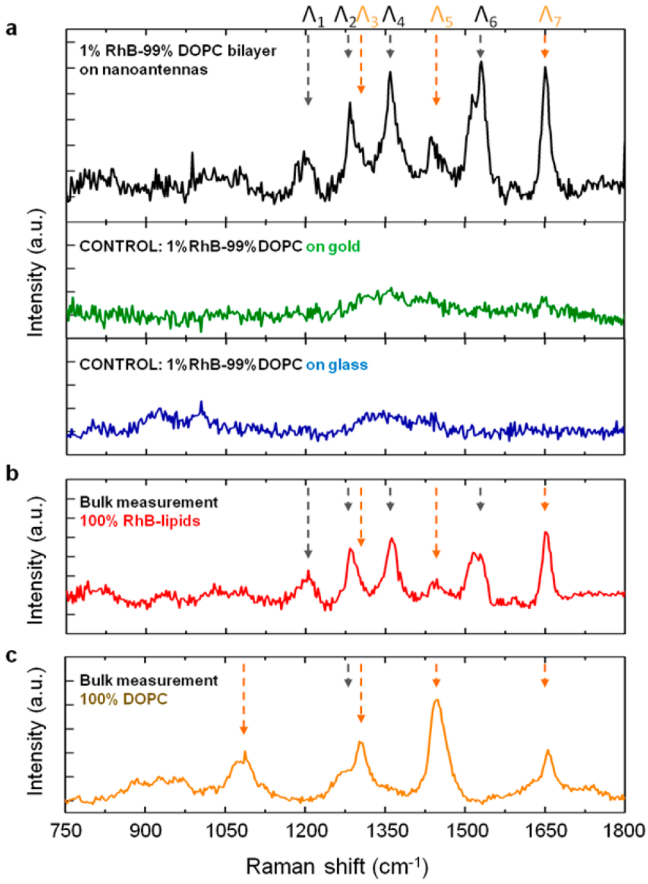

Figure 3. (a) Raman spectrum of L-RhB on the nanoantenna array and control measurements on gold and on glass for comparison. Upper part: Spectra of supported DOPC membranes with a 1% concentration of RhB moluecules on the nanoantenna array (black curve). Raman peaks are located at: Λ_1 = 1200 cm^{-1}, Λ_2 = 1270 cm^{-1}, Λ_3 = 1285 cm^{-1}, Λ_4 = 1360 cm^{-1}, Λ_5 = 1435 cm^{-1}, Λ_6 = 1530 cm^{-1}, and Λ_7 = 1650 cm^{-1}. Raman peaks that could be assigned to RhB are indicated by a dark gray arrow and Raman peaks corresponding to DOPC are indicated by an orange arrow. A control measurement was performed on a gold patch on the same sample in order to exclude any deviation of the Raman signal intensity due to sample preparation (e.g., roughness of the gold film, sample contamination). The green spectrum also shows that no Raman signal is expected from lipid molecules that are just randomly adsorbed to the gold film. Also, no Raman signal was obtained just from a supported membrane on glass (blue curve). All graphs are an average from over over 45 SERS spectra that were measured at different regions on the sample. (b) Bulk measurement of a RhB-lipid solution (conc. One mg/mL) and (c) bulk measurements of a 100% DOPC sample were performed to identify the Raman peaks measured on the bilayer membrane.

Table 1. Raman Shifts Associated with RhB and DOPC

Raman shift (cm^{-1})	assignment	ref
1200	L-RhB (aromatic C−H bending)	32,33
1285	L-RhB (C−C bridge-bands stretching)	32,33
1360	L-RhB (aromatic C−C stretching)	32,33
1435	L-RhB/DOPC (CH2 bending)	32,34
1530	L-RhB	32,33
1650	L-RhB (aromatic C−C stretching)/DOPC (C═C stretching)	32−34

dx.doi.org/10.1021/am5023418 | ACS Appl. Mater. Interfaces 2014, 6, 8947−8952

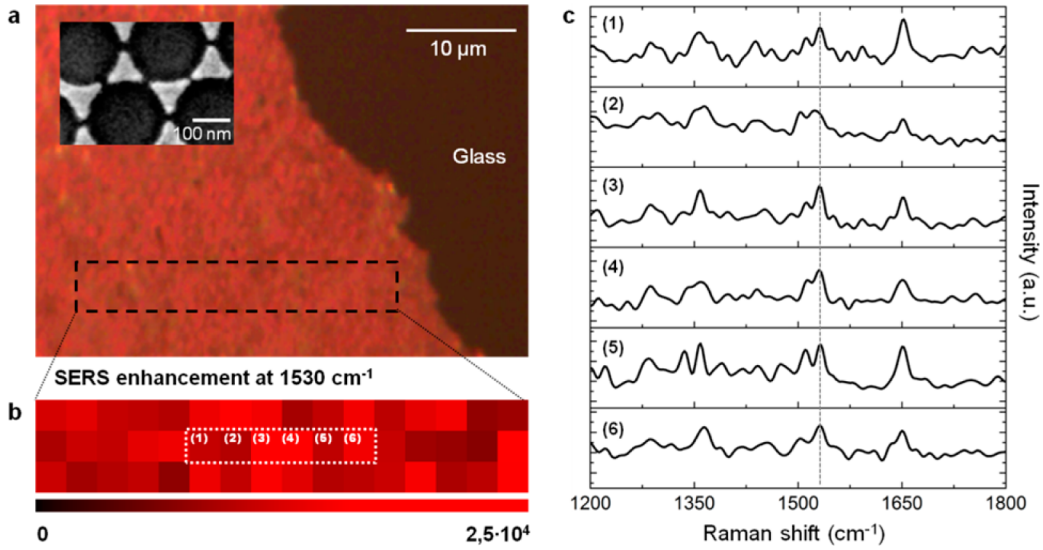

Figure 4. (a) Optical microscope image of a substrate that is covered with a bilayer made from 99% DOPC doped with a 1% fraction of L-RhB molecules (in EPI illumination). The strong scattering of the triangle array (inset: SEM image) appears in red, whereas the dark region indicates the bare glass surface. (b) Full map of the Raman enhancement at 1530 cm^{-1} displays the homogeneity of the overall Raman signal. (c) Raman spectra taken at single points of the Raman map marked in b.

for a spot diameter of 1.5 μm (fwhm) assuming a perfect, defect-free bowtie array. However, not all illuminated bowties contribute equally to the SERS signal. SEM analysis of the triangle array revealed that about 30% of the bowties are connected at their tips due to lattice defects in the polystyrene particle mask. The affected nanoantennas may not contribute to the SERS signal because of their presumably significantly red-shifted plasmon resonance. Finally, the polarization dependence of the LSP excitation leads to differences in the SERS contribution according to the bowtie orientation with respect to the laser polarization (see the Supporting Information, Figure S5). Comparison of the bulk solution measurements of the L-RhB lipids to resonant Raman studies at much higher excitation power and long integration times of black membranes[12] yields that the Raman scattering cross section of the L-RhB molecules is only 3×10^2 higher than the one of unlabeled lipid molecules at resonant excitation (see the Supporting Information for details). This also presents a benchmark for the further improvement our method for enabling SERS measurements of unlabeled membrane constituents at low concentration.

In conclusion, the incorporation of plasmonic nanoantennas with fluid supported membranes for SERS spectroscopy renders it possible to measure the chemical fingerprint of molecules that are freely diffusing in a bilayer membrane. The molecules of interest are detected as they sequentially pass through the "hot-spot" regions presented by the bowtie antenna array without static entrapment of the bilayer. In such a configuration, the membrane can also be envisioned as scaffold to specifically bind molecules such as proteins or small antibodys from solution and detect them by the nanoantenna array as these molecules sequentially pass the plasmonic hot-spot region. We observed a SERS enhancement factor in the order of 1×10^4, which was suitable to detect a one percent fraction of Rhodamine lipids in an otherwise pure DOPC bilayer membrane.

As mentioned earlier, supported membranes have been demonstrated to be suitable as a platform for experiments on living cells. The plasmonic nanoantennas would thereby represent both: a physical barrier to probe and direct receptor cluster movement on a cell-bilayer interface and a tool to investigate these cell−membrane interactions by means of spectroscopy. The applicability of this experimental platform for live-cell investigations could potentially provide useful information about the chemical nature of cell−cell interaction and communication and will be investigated in the near future.

■ ASSOCIATED CONTENT

Supporting Information

Materials and Methods, FDTD calculation details, transmission spectra of the nanotriangle arrays, FDTD calculations of polarization effects, FRAP measurement of the lipid membrane in between the nanotriangle array. This material is available free of charge via the Internet at http://pubs.acs.org/.

■ AUTHOR INFORMATION

Corresponding Author

*E-mail: t.lohmueller@lmu.de.

Notes

The authors declare no competing financial interest.

■ ACKNOWLEDGMENTS

By the DFG through the Nanosystems Initiative Munich (NIM) and through the Collaborative research center (SFB1032), Project A8 is gratefully acknowledged.

■ ABBREVIATIONS

TIR, total internal reflection
LSP, localized surface plasmons
PS, polystyrene
SLB, supported lipid bilayer
L-RhB, 18:1 LISS Rhod PE
fwhm, full width at half-maximum
SEM, scanning electron microscope

REFERENCES

(1) Bretscher, M. S. Asymmetrical Lipid Bilayer Structure for Biological Membranes. *Nature. New Biol.* **1972**, *236*, 11−12.

(2) Groves, J. T.; Kuriyan, J. Molecular Mechanisms in Signal Transduction at the Membrane. *Nat. Struct. Mol. Biol.* **2010**, *17*, 659−665.

(3) Singer, S. J.; Nicolson, G. L. The Fluid Mosaic Model of the Structure of Cell Membranes. *Science* **1972**, *175*, 720−731.

(4) Axelrod, D. Total Internal Reflection Fluorescence Microscopy in Cell Biology. *Traffic* **2001**, *2*, 764−774.

(5) Crane, J. M.; Kiessling, V.; Tamm, L. K. Measuring Lipid Asymmetry in Planar Supported Bilayers by Fluorescence Interference Contrast Microscopy. *Langmuir* **2005**, *21*, 1377−1388.

(6) Wong, A. P. Molecular Topography Imaging by Intermembrane Fluorescence Resonance Energy Transfer. *Proc. Natl. Acad. Sci. U.S.A.* **2002**, *99*, 14147−14152.

(7) García-Sáez, A. J.; Carrer, D. C.; Schwille, P. Fluorescence Correlation Spectroscopy for the Study of Membrane Dynamics and Organization in Giant Unilamellar Vesicles. In *Liposomes*; Weissig, V., Ed.; Humana Press: Totowa, NJ, 2010; Vol. *606*, pp 493−508.

(8) Guerquin-Kern, J.-L.; Wu, T.-D.; Quintana, C.; Croisy, A. Progress in Analytical Imaging of the Cell by Dynamic Secondary Ion Mass Spectrometry (SIMS Microscopy). *Biochim. Biophys. Acta BBA-Gen. Subj.* **2005**, *1724*, 228−238.

(9) Schultz, Z. D.; Levin, I. W. Vibrational Spectroscopy of Biomembranes. *Annu. Rev. Anal. Chem.* **2011**, *4*, 343−366.

(10) Schrader, B.; Bougeard, D. *Infrared and Raman Spectroscopy Methods and Applications*; VCH: Weinheim, Germany, 1995.

(11) Kato, Y.; Takuma, H. Absolute Measurement of Raman-Scattering Cross Sections of Liquids. *J. Opt. Soc. Am.* **1971**, *61*, 347.

(12) Lee, C.; Bain, C. D. Raman Spectra of Planar Supported Lipid Bilayers. *Biochim. Biophys. Acta BBA-Biomembr.* **2005**, *1711*, 59−71.

(13) Lhert, F.; Blaudez, D.; Heywang, C.; Turlet, J.-M. Free-Standing Black Films: An Alternative to Langmuir Monolayers for the Study by Raman Spectroscopy of Peptide−Phospholipid Interaction in Ultra-thin Films. *Langmuir* **2002**, *18*, 512−518.

(14) Sharonov, A.; Bandichhor, R.; Burgess, K.; Petrescu, A. D.; Schroeder, F.; Kier, A. B.; Hochstrasser, R. M. Lipid Diffusion from Single Molecules of a Labeled Protein Undergoing Dynamic Association with Giant Unilamellar Vesicles and Supported Bilayers. *Langmuir* **2008**, *24*, 844−850.

(15) Schuck, P. J.; Fromm, D. P.; Sundaramurthy, A.; Kino, G. S.; Moerner, W. E. Improving the Mismatch between Light and Nanoscale Objects with Gold Bowtie Nanoantennas. *Phys. Rev. Lett.* **2005**, *94*.

(16) Nordlander, P.; Oubre, C.; Prodan, E.; Li, K.; Stockman, M. I. Plasmon Hybridization in Nanoparticle Dimers. *Nano Lett.* **2004**, *4*, 899−903.

(17) LeRu, E. C.; Blackie, E.; Meyer, M.; Etchegoin, P. G. Surface Enhanced Raman Scattering Enhancement Factors: A Comprehensive Study. *J. Phys. Chem. C* **2007**, *111*, 13794−13803.

(18) Sackmann, E. Supported Membranes: Scientific and Practical Applications. *Science* **1996**, *271*, 43−48.

(19) Lin, W.-C.; Yu, C.-H.; Triffo, S.; Groves, J. T. Supported Membrane Formation, Characterization, Functionalization, and Patterning for Application in Biological Science and Technology. In *Current Protocols in Chemical Biology*; Arkin, A. P., Mahal, L., Romesberg, F., Shah, K., Shamu, C., Thomas, C., Eds.; John Wiley & Sons: Hoboken, NJ, 2010.

(20) Groves, J. T.; Ulman, N.; Boxer, S. G.; Micropatterning Fluid, Lipid Bilayers on Solid Supports. *Science* **1997**, *275*, 651−653.

(21) Nabika, H.; Sasaki, A.; Takimoto, B.; Sawai, Y.; He, S.; Murakoshi, K. Controlling Molecular Diffusion in Self-Spreading Lipid Bilayer Using Periodic Array of Ultra-Small Metallic Architecture on Solid Surface. *J. Am. Chem. Soc.* **2005**, *127*, 16786−16787.

(22) Lohmüller, T.; Triffo, S.; O'Donoghue, G. P.; Xu, Q.; Coyle, M. P.; Groves, J. T. Supported Membranes Embedded with Fixed Arrays of Gold Nanoparticles. *Nano Lett.* **2011**, 111011130133001.

(23) Groves, J. T.; Ulman, N.; Cremer, P. S.; Boxer, S. G. Substrate−Membrane Interactions: Mechanisms for Imposing Patterns on a Fluid Bilayer Membrane. *Langmuir* **1998**, *14*, 3347−3350.

(24) Kashimura, Y.; Furukawa, K.; Torimitsu, K. Electrostatic Control of Lipid Bilayer Self-Spreading Using a Nanogap Gate on a Solid Support. *J. Am. Chem. Soc.* **2011**, *133*, 6118−6121.

(25) Fischer, U. C.; Zingsheim, H. P. Submicroscopic Pattern Replication with Visible Light. *J. Vac. Sci. Technol.* **1981**, *19*, 881.

(26) Haynes, C. L.; Van Duyne, R. P. Nanosphere Lithography: A Versatile Nanofabrication Tool for Studies of Size-Dependent Nanoparticle Optics. *J. Phys. Chem. B* **2001**, *105*, 5599−5611.

(27) Jacobs, R. E.; White, S. H. The Nature of the Hydrophobic Binding of Small Peptides at the Bilayer Interface: Implications for the Insertion of Transbilayer Helices. *Biochemistry* **1989**, *28*, 3421−3437.

(28) Fischer, H.; Martin, O. J. F. Engineering the Optical Response of Plasmonic Nanoantennas. *Opt. Express* **2008**, *16*, 9144−9154.

(29) Moskovits, M. Surface-Enhanced Raman Spectroscopy: A Brief Retrospective. *J. Raman Spectrosc.* **2005**, *36*, 485−496.

(30) Lohmüller, T.; Iversen, L.; Schmidt, M.; Rhodes, C.; Tu, H.-L.; Lin, W.-C.; Groves, J. T. Single Molecule Tracking on Supported Membranes with Arrays of Optical Nanoantennas. *Nano Lett.* **2012**, *12*, 1717−1721.

(31) Koppel, D. E.; Sheetz, M. P.; Schindler, M. Matrix Control of Protein Diffusion in Biological Membranes. *Proc. Natl. Acad. Sci. U.S.A.* **1981**, *78*, 3576−3580.

(32) Vo-Dinh, T.; Allain, L. R.; Stokes, D. L. Cancer Gene Detection Using Surface-Enhanced Raman Scattering (SERS). *J. Raman Spectrosc.* **2002**, *33*, 511−516.

(33) Zhang, J.; Li, X.; Sun, X.; Li, Y. Surface Enhanced Raman Scattering Effects of Silver Colloids with Different Shapes. *J. Phys. Chem. B* **2005**, *109*, 12544−12548.

(34) Cherney, D. P.; Conboy, J. C.; Harris, J. M. Optical-Trapping Raman Microscopy Detection of Single Unilamellar Lipid Vesicles. *Anal. Chem.* **2003**, *75*, 6621−6628.